SERS detection via individual bow-tie nanoantennas integrated in Si_3N_4 waveguides

Javier Losada, Ali Raza, Stéphane Clemmen, Aina Serrano, Amadeu Griol, Roel Baets and Alejandro Martínez, *Senior Member, IEEE*

***Abstract*—Plasmonic resonances in metallic nanostructures provide a way for broadband enhanced light-matter interaction in subwavelength regions, which can be used to boost a variety of physical phenomena, notably including Raman scattering. Such nanostructures can be integrated on silicon chips and driven via dielectric waveguides, which may improve the performance of photonic integrated circuits in terms of foot-print, efficiency, sensitivity or power consumption, amongst other figures of merit. Here, we show that an isolated plasmonic nanoantenna can be efficiently integrated into a silicon nitride waveguide to detect surface-enhanced Raman scattering (SERS) spectra from molecular monolayers. We study numerically and experimentally two different configurations, both enabling the recording of Raman spectra at the output: nanoantenna on top of the waveguide and nanoantenna inserted in a subwavelength gap built in the waveguide. We also compare both configurations, which may pave the way towards massive integration of SERS devices for lab-on-a-chip applications.**

***Index Terms*— Nanophotonics, Plasmons, Raman Scattering, Silicon photonics.**

I. Introduction

Integration of subwavelength-sized plasmonic nanostructures in silicon waveguides has received a considerable interest in the past few years. The main reason is that this hybrid plasmonic-photonic approach [1] reunites the best of two worlds: on one side, the extreme optical properties of plasmonic nanostructures enabling a variety optical functionalities (sensing, modulation, non-linear processing) at low power and in sub-micron foot-prints; on the other side, the possibility of massive fabrication of photonic integrated circuits (PICs) using silicon-compatible technologies. A paradigmatic example of such a hybrid approach is the recent demonstration of a plasmonic electro-optic modulator integrated on a silicon waveguide which beats its dielectric counterparts in terms of speed, power consumption and foot-print [2].

One of the possible plasmonic structures to be integrated in silicon-based PICs is a metallic nanoantenna [3] supporting a localized surface plasmon resonance (LSPR) either in the near-infrared [4] or in the visible regime [5]. Either silicon or silicon nitride (Si_3N_4) waveguides are respectively chosen for each wavelength regime to ensure strong confinement in the waveguide core together with low propagation losses. In the simplest approach, plasmonic nanoantennas can be placed on top of the dielectric waveguides so that their excitation arises from the coupling between the evanescent part of the waveguide mode (usually, the fundamental TE-like mode) and the nanoantenna LSPR. This approach, which allows for both exciting the nanoantenna via the guided field and collecting the radiation that it scatters back to the coupled waveguide, has led to different interesting experimental results [4]-[11]. However, the weak coupling (~10% at most) between the waveguide mode and the LSPR makes typically necessary to include a set of nanoantennas in order to observe a large contrast ratio at the waveguide output [5],[7]. The requirement for several antenna is a limiting factor obviously when probing single particles but also because it increases the propagation length into the Si_3N_4 core resulting in a much higher photon background radiation [10].

Plasmonic nanostructures play a key role in surface-enhanced Raman scattering (SERS), since the strong field localization in subwavelength volumes boost the efficiency of the Raman process by orders of magnitude [12]-[14]. Recently, the collection of SERS spectra from nanoantennas integrated on top of Si_3N_4 waveguides has been demonstrated, first by means of an array of nanoantennas to increase the amount of Raman scattering collected by the waveguides [15] and afterwards by means of a single nanoantenna by reducing the background noise in a backscattering detection scheme with short waveguide lengths [16].

Still, there is room for improvement, mainly in terms of excitation and collection efficiency, in the way towards single-molecule on-chip SERS. A possible way to increase the coupling efficiency between the nanoantenna and the guided

Manuscript received July 31, 2018. (A. M. acknowledges support from the Spanish Ministry of Economy and Competiveness (MINECO) under grants TEC2014-51902-C2-1-R and TEC2014-61906-EXP. A. R., S. C. and R. B. acknowledges funding by ERC Grant InSpectra and the FWO Belgium. S. C. also acknowledges the financial support from the F.R.S-FNRS.)

J. L., A. S., A. G. and A. M. are with the Nanophotonics Technology Center, Universitat Politècnica de València, Camino de Vera s/n, 46022, Valencia (Spain). (corresponding author's phone: +34 963877000 88115; fax: +34 96 387 78 27; e-mail: amartinez@ntc.upv.es).

A. R., S. C. and R. B. are with Photonics Research Group, INTEC Department, Ghent University-imec, Technologiepark-Zwijnaarde, 9052 Ghent and Center for Nano- and Biophotonics, Ghent University, Belgium. S.C. is also with Laboratoire d'information quantique, Université Libre de Bruxelles, 1050 Bruxelles, Belgium

J. L. and A. R. have equally contributed to this paper.

mode results from placing the nanoantenna in a subwavelength gap created in the waveguide, so that the nanoantenna is perfectly aligned with the waveguide optical axis [17]. In this approach, it can be considered that the nanoantenna is illuminated by a near-field probe (the waveguide facet) so the optical power delivered to the nanoantenna should be higher than in the on-top nanoantenna approach, thus enhancing the efficiency of the Raman process. However, this waveguide-gap approach has not been employed so far in SERS.

In this work, we demonstrate SERS via isolated bow-tie Au nanoantennas integrated in Si_3N_4 waveguides using the two previous approaches: antenna on top and antenna in the gap. We show that both approaches enable to record SERS spectra but the gap approach performs better, which is supported by numerical results.

II. Numerical Study

Figure 1 shows a sketch of the two configurations under study: nanoantenna on top of the waveguide (Fig. 1(a)) and nanoantenna inserted in a subwavelength gap in the waveguide (Fig. 1(b)). For simplicity, we term these configurations C1 and C2, respectively. In both cases, we consider Si_3N_4 waveguides with a rectangular cross-section (w=700 nm and t=220 nm) on a silica substrate and bow-tie nanoantennas made of gold (Au).

There are two key parameters to model the performance of the structures in SERS [15]: the Raman enhancement factor and the β-factor. The Raman enhancement factor EF_R characterizes the excitation efficiency of the Raman centers. At a certain position, it can be obtained as $EF_R = I(\lambda_P)I(\lambda_S)$, where I stands for the optical intensity (or square of the electric field modulus $|E|^2$ in that position) and λ_P and λ_S are respectively the pump and Stokes wavelengths. Since plasmonic resonances are generally broad (optical Q factor ≈ 10 or bandwidths ≈ 100 nm at near infrared wavelengths), the intensity enhancement I at the pump and Stokes wavelengths are quite similar so EF_R is typically considered to be proportional to $|E|^4$ (the so-called 'E^4 law' [13],[14]). In Ref. [15] the field normalization was carried out by comparing the field at the nanoantenna position

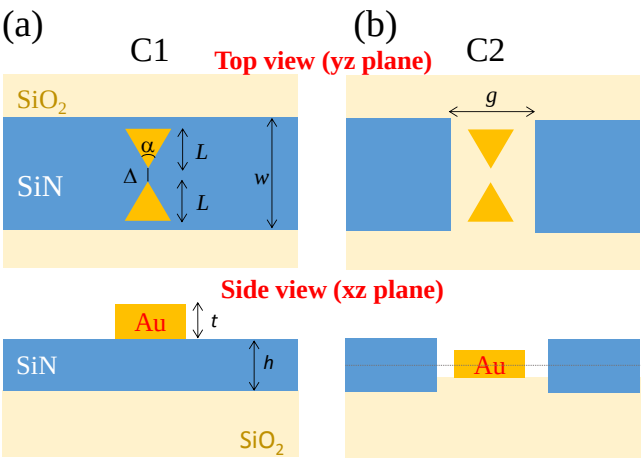

Fig. 1. Sketch of the two configurations under study: (a) The nanoantenna is placed on top of the waveguide so that its excitation is mediated by evanescent field coupling (C1); (b) The nanoantenna is placed in a gap created in the waveguide and aligned with the optical axis (C2).

(evanescent field region over the top waveguide boundary) with and without nanoantenna. Since the nanoantennas are placed in different positions for each configuration, we will use the electric field at the center of the waveguide for normalization to ensure a fair comparison between both approaches. On the other hand, the β-factor models the amount of the Raman radiation that is coupled to the guided mode, and can be obtained as $\beta=P_{TE}/P_{rad}$, where P_{rad} is the total power radiated by a Raman center and P_{TE} is the power of the output guided mode. Noticeably, the analytical model developed in Ref. [15] for both parameters cannot be applied to C2, so here we use numerical simulations to compare the performance of both approaches.

We performed full-vectorial electromagnetic simulations using the software *CST Microwave Studio*. For both configurations we followed the same procedure: We used a non-dispersive refractive index of n_{SiN} = 1.99 for the waveguide core, n_{SiO2} = 1.45 for the silica (SiO_2) undercladding and n_{air} = 1 for the air top cladding. We considered a thin layer of titanium as an adhesion layer between SiO_2 and Au. The metal stack thicknesses were fixed to t_{Ti} = 2 nm and t_{Au} = 30 nm, so t = 32 nm. An additional surface layer with thickness t_{MM} = 1 nm and index n_{MM} = 3 was used to model the molecular monolayer placed on top of the sample. The nanoantenna region (including the titanium adhesion layer and the monolayer) was meshed with a uniform mesh of 0.5 nm in the plane of the nanoantenna (yz-plane) and 1 nm in the x-direction. A mesh refinement to 0.5 nm is applied in regions where the thickness in the x-direction was ≤ 1 nm.

To calculate the intensity enhancement I, we placed an electric field monitor in the middle of the gap formed by the two bow-tie arms at a height of 15 nm. For the β-factor calculations, we considered a fixed dipole emitter source positioned near the antenna surface, centered in the bow-tie gap and at a height of 15 nm over the surface (this means, 45 nm over the substrate layer). P_{rad} can then be calculated using a 3D power monitor whose boundaries are in the far field of the dipole source. P_{TE} can be simultaneously determined using a monitor that extracts the power carried by the TE mode.

The nominal parameters of the C1 design were directly extracted from Ref. [15]: α= 60.51º, Δ= 20 nm, t = 30 nm and L=120 nm. C2 was designed to get the highest value of $EF(\lambda_P)^2$ in the wavelength region used in the experiments (around 780 nm). After the optimization step, the dimensions of the C2 nanoantenna are α= 64º, Δ = 35 nm, t= 30 nm and L=120 nm, for a waveguide gap of g = 200 nm.

Figure 2 depicts a comparison between both nominal designs, in terms of both $I(\lambda_P)$ (a) and the β-factor (b). It can be clearly seen that C2 performs better than C1 since both the Raman centers are excited more efficiently and the Raman excitation is more efficiently captured by the output waveguide. Especially, C2 provides a much higher field enhancement at the bowtie gap, as also shown in the electric field snapshots shown in Fig. 3. This can be attributed to two

main reasons: first, because the plasmonic resonance seems to be red-shifted in C1; and second because the interaction between the guided fields is higher in C2 than in C1. As a result of the inaccuracies in the fabrication process, the dimensions of the real samples were different from the nominal designs (see Section III and, particularly, Fig. 4). Still, C2 is expected to be more efficient than C1, even though the performance of C1 could be certainly improved by designing the antenna to resonate closer to the pump wavelength.

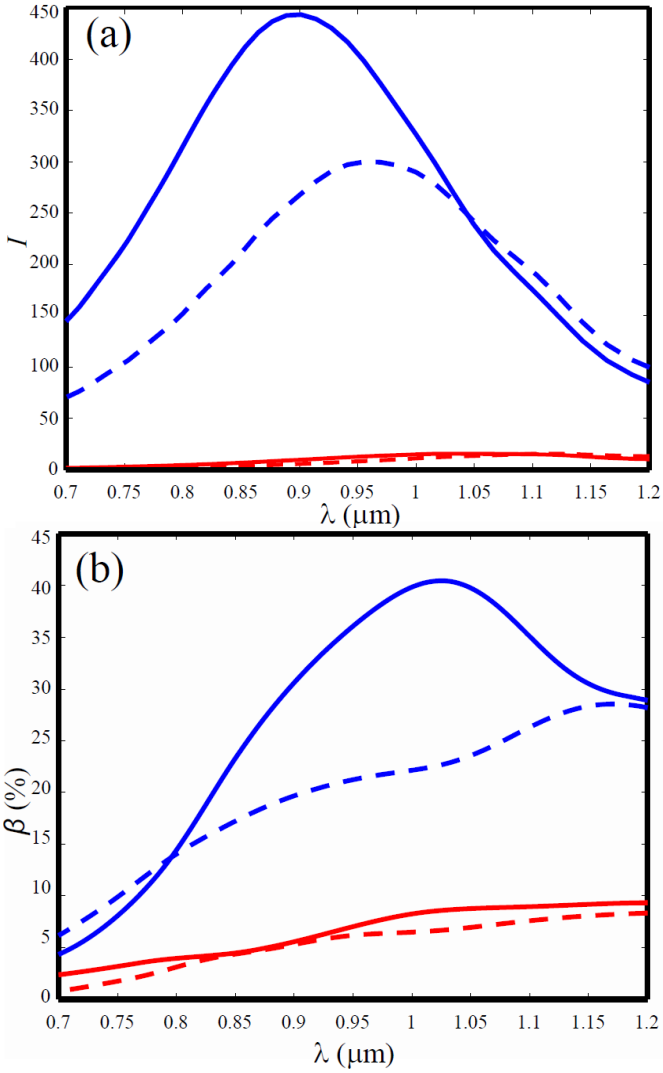

Fig. 2. Intensity enhancement factor $I(\lambda)$ (a) and β-factor (b) for both designs, C1 (red) and C2 (blue). Solid lines describe the response for ideally designed systems, whilst dahsed lines show the response for the final fabricated systems (taking into account fabrication deviations).

III. Fabrication

The samples for both C1 and C2 configurations were fabricated using standard silicon technology. As a starting material, a 200 mm Si wafer containing a stack of 2.3 ± 0.1 μm thick high-density plasma chemical vapor deposition SiO_2 and 220 nm thick plasma enhanced chemical vapor deposition (PECVD) Si_3N_4 is used [18]. First, the Si_3N_4 waveguides (with the gap for C2 samples) were fabricated. The fabrication

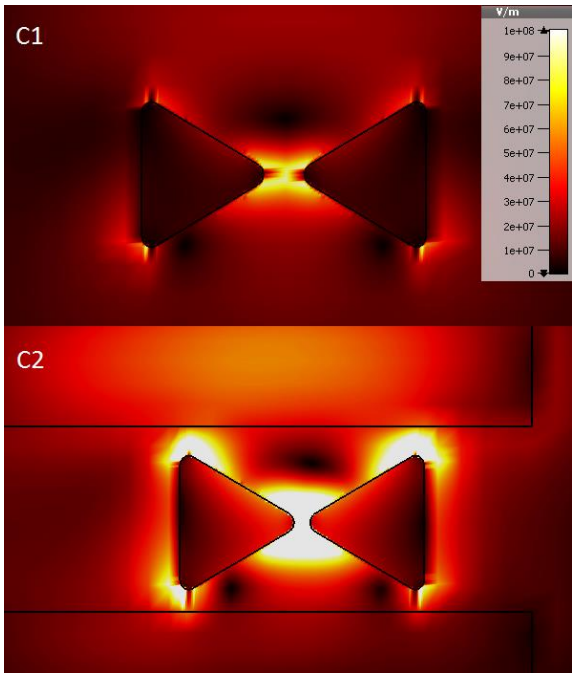

Fig. 3. Snapshots of the electric field at λ=876 nm (roughly corresponding to the main Raman peak of the substance used in the experiments) around the nanoantenna region for both the C1 (top) and C2 (bottom) configurations. In both cases, the guided power is the same. The colorbar applies to both parts of the figure.

process was based on an electron-beam direct-writing process performed on a 100-nm-thick poly(meth)acrylates (PMMA 905 K) resist film. The mentioned electron-beam exposure, performed with a Raith150 tool, was optimized in order to reach the required dimensions employing an acceleration voltage of 10 KeV and an aperture size of 30 μm. After developing the PMMA resist using a mixture of IPA+MIBK, and in order to have an etching metal mask, a 20 nm chromium layer was evaporated prior to a lift-off process. Then, the waveguide patterns were transferred into the Si_3N_4 samples employing an optimized Inductively Coupled Plasma-Reactive Ion Etching process with fluoride gases. Finally, the remaining chromium layer was removed by using chromium etchant dissolution. For the C2 samples, an extra PECVD step for silica deposition (around 100nm) was required in order to ensure the right height alignment between the antenna and the waveguide axis (see Fig. 1(b)).

Once the waveguides were fabricated, the Au bow-tie structures were placed on the waveguides as well as in the middle of the waveguide gaps by means of a second e-beam lithography process performed with the Raith150 tool prior to a new metal evaporation (30 nm of gold plus 3 nm of titanium for adhesion enhancement) and lift-off process. To ensure the right placement of the bowties, alignment marks, created in the previous Si_3N_4 etching level, and an iterative exposure process were used. Four samples were fabricated (one for C1 and three for C2) all of them containing a waveguide without nanoantenna for calibration purposes and seven waveguides with nanoantenna. Figure 4 shows SEM images of some of the fabricated samples. As mentioned in section II, the shape of

the fabricated bow-ties was a little bit different from the nominal bow-tie geometry because of fabrication inaccuracies. Indeed many of the bow-ties were not well formed (so they were not useful for characterization) and their bow-tie aperture was different from the nominal one as shown in Fig. 3(a) and (b). Moreover, in some of the samples the bow-tie gap was completely closed (Fig. 3(c)). The dimensions for fabricated antennas used in measurements were: α= 56.15º, Δ = 44 nm, t= 30 nm and L=131.5 nm , (C1, Fig. 4(a)), and α= 59.71º, Δ= 35 nm, t = 30 nm and L=135 nm (C2, Fig. 4(b)). In addition, there is a certain misalignment with respect to the optical axis, which also was accounted for in the simulations. Still, we were able to excite the nanoantenna resonances as shown in Section IV.

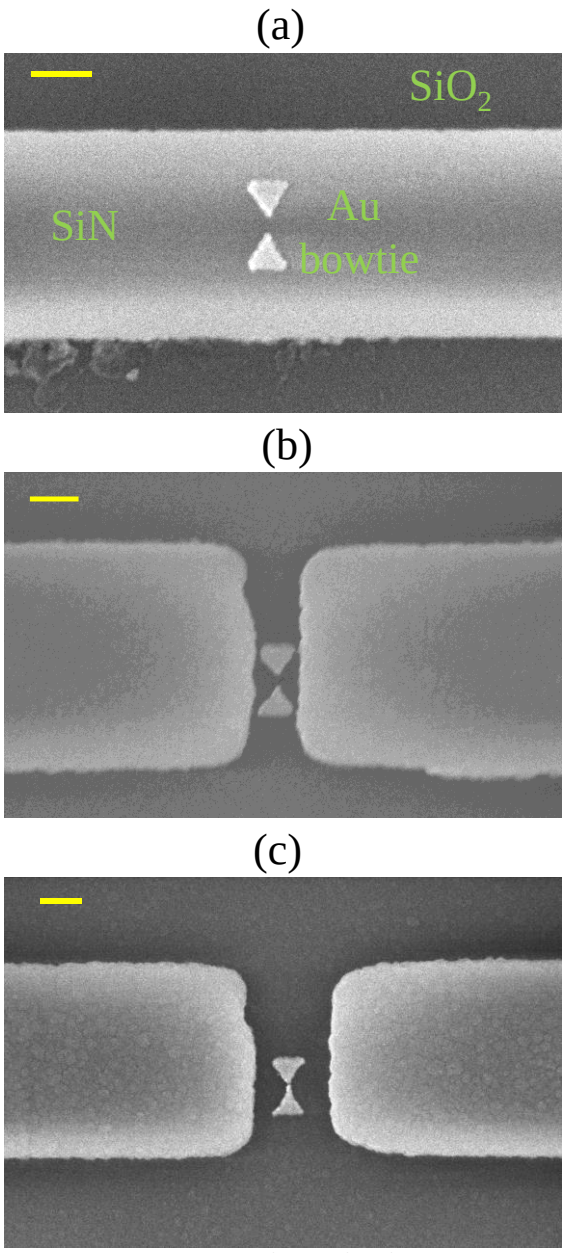

Fig. 4. Scanning Electron Images of some of the fabricated samples: C1 in (a), with Δ=44 nm; C2 in (b) with Δ=35 nm and (c) with Δ=0 nm (the bow-tie gap was not opened). The yellow line stands for 200 nm.

For SERS measurements, the fabricated chips were first cleaned using acetone + IPA + DI-water followed by O_2 plasma. Then 4-nitrophenol (pNTP) molecules in the form of a monolayer were bound to the plasmonic nanoantenna by immersing the chip in a 1mM solution of pNTP in ethanol. After an overnight immersion, chips were thoroughly washed with ethanol and DI-water to remove the unbind pNTP molecules.

IV. Experimental Results

We performed the SERS measurements using a commercial confocal Raman microscope (WITEC Alpha300R+). The schematic of the experimental setup is presented in Fig. 5. The inset shows the input laser spot and the scattering from the single antenna. A λ_P = 785 nm excitation diode laser (Toptica XTRA II) is used as a pump source. The chip was placed underneath the objective (40 ×, 0.63 NA) i.e. TE mode of Si_3N_4 waveguide is excited via end-fire coupling. A low pump power of 1 mW (before objective) is used to avoid any material damage and subsequent photoreduction of pNTP. The coupling into the waveguide was optimized by looking simultaneously at the waveguide scattering using the top camera as well as at the expected 1339 cm^{-1} pNTP peak. All the Raman spectra were recorded with 1 sec integration time. The loss of the Si_3N_4 waveguide measured using cut back method is 3.2 ± 0.9 dB/cm. The coupling loss measured from the chip containing C1 and C2 configuration is 3.2 ± 0.5 and 5.0 ± 0.4 dB/facet. Further details about the experimental setup can be read from [16].

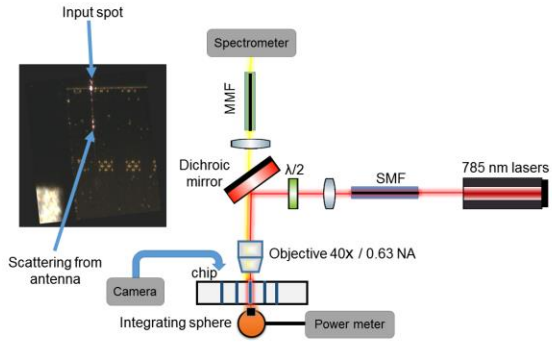

Fig. 5. The schematic of the setup used for SERS measurements from nanoantennas integrated Si_3N_4 waveguides. The inset shows the input spot and the scattering from the single nanoantenna.

The measurement results are presented in Fig 6. Each spectrum is normalized by the coupling efficiencies to assure same pump power for both configurations. No NTP peak can be seen in the Raman spectrum measured from a reference waveguide (black). However, a strong NTP spectrum is present in the signal recorded from the waveguide functionalized with a single antenna (red). Apart from the expected pNTP Raman modes, a spurious Raman like background generated from the Si_3N_4 waveguide [10] is observed in all spectra. In the first set of measurements, the chip containing a set of waveguides with the bow-tie on top (C1) is measured. For the best waveguide-antenna system (Fig.

3(a)) the Raman peak of the 1339 cm^{-1} mode ($\boldsymbol{\nu}_s$ (NO_2)) is visible in Fig 6(a). However, due to the low excitation and collection efficiency (β-factor), no other Raman modes are present. In the second set of the measurements, the set of samples with antennas in the gap (C2) was explored. The same pump power, integration time and CCD setting were used. As shown in Fig 6(b), aside from 1339 cm^{-1} Raman modes, two more peaks at 1076 cm^{-1} and 1580 cm^{-1} (benzene ring vibrations) also appear in the Raman spectra. The higher noise in Fig 6(b) is attributed to higher coupling loss. In Fig 6(c), we compare the Raman signal strength measured from both antenna configurations. For the same pump power and integration time, the Raman signal recorded for C2 is at least three times stronger than in C1, where both antennas geometries were optimized for highest signal strength.

These experimental results are supported by the numerical predictions: being the intensity enhancement and the β-factor about two and one orders of magnitude higher in C2 than in C1, we could expect a much better resolved Raman spectrum in C2. In this sense, it is worth mentioning that C1 is far from being optimized and the bowtie plasmonic resonance is redshifted beyond 1 μm, so in an optimum configuration with the resonance close to the pump laser the C1 structure would enable to record also all the Raman peaks, as shown in [16].

V. Conclusion

In this work, we have demonstrated that the marriage between silicon photonics and plasmonics may give rise to new devices for advanced spectroscopy. In particular, single plasmonic nanoantennas with a sub-micron square foot-print, well below what can be achieved using dielectric structures, can enormously concentrate incoming guided fields to excite Raman centers whose emitted radiation is also efficiently collected by output waveguides.

Next steps should include the increase of the field localization (higher values of I) via narrower gaps (< 10 nm) in the nanoantenna, which should lead to single-molecule spectroscopy [19] on silicon chips. Such narrowing could be performed by alternative methods in which the gap is not defined lithographically but by self-assembly, as recently demonstrated in plasmonics picocavities following a nanoparticle-on-mirror structure [20]. Ways for enhancing the collection of the Raman radiation by the output waveguide are to be addressed, especially for the C2 configuration where the distance from the nanoantenna to the output waveguide facet should be as small as possible in order to capture the maximum amount of emitted radiation.

In the way towards commercialization, CMOS compatibility should also be considered. In this case, the replacement of Au (not CMOS compatible) by CMOS-compatible plasmonic materials [21] such as titanium nitride [22] or copper [23] would be mandatory. By additionally using multiple waveguides with integrated antennas, which could be simultaneously excited by a single laser, it would be feasible to perform Raman spectroscopy of multiple substances in ultra-compact and low-cost SERS chips.

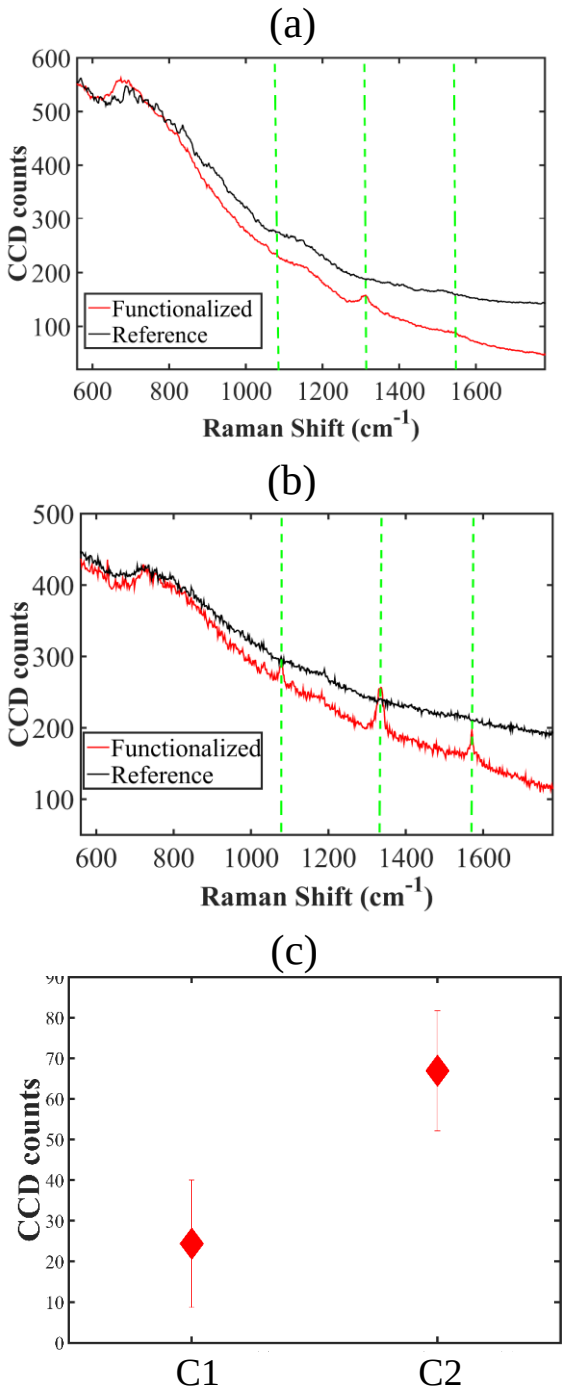

Fig. 6. The Raman spectrum measured from the waveguides functionalized with single antenna for C1 (a) and C2 (b). The green dotted line represents the NTP Raman modes i.e. 1080, 1339 and 1575 cm^{-1}. (c) The CCD counts corresponding to 1339 cm^{-1} Raman mode of NTP.

Acknowledgment

The authors would like to thank Prof. Andre Skirtach (UGent, Belgium) for his support in experiments. The authors would also thank Dr. Frédéric Peysken (UGent, Belgium / Quantum Photonics Laboratory, RLE, MIT, USA) for useful discussion.

REFERENCES

[1] F. J. Rodríguez-Fortuño, A. Espinosa-Soria, and A. Martínez, "Exploiting metamaterials, plasmonics and nanoantennas concepts in silicon Photonics," *J. Opt.* vol. 18, pp. 123001-123014, 2016.

[2] C. Haffner et al., "Low-loss plasmon-assisted electro-optic modulator," *Nature*, vol. 556, pp. 483–486, 2018.

[3] L. Novotny and N. F. van Hulst, "Antennas for light," *Nat. Photonics* vol. 5, pp. 83–90, 2011.

[4] I. Alepuz-Benache, C. García-Meca, F. J. Rodríguez-Fortuño, R. Ortuño, M. Lorente-Crespo, A. Griol, and A. Martínez: Strong magnetic resonance of coupled aluminum nanodisks on top of a silicon waveguide, *Proc. SPIE* vol. 8424, p. 84242J, 2012.

[5] F. Peyskens, A. Z. Subramanian, P. Neutens, A. Dhakal, P. Van Dorpe, N. Le Thomas, and R. Baets, "Bright and dark plasmon resonances of nanoplasmonic antennas evanescently coupled with a silicon nitride waveguide," *Opt. Express*, vol. 23, no. 3, pp. 3088–3101, 2015.

[6] F. Bernal Arango, A. Kwadrin, and A. F. Koenderink, "Plasmonic antennas hybridized with dielectric waveguides," *ACS Nano*, vol. 6, no. 11, pp. 10156–10167, 2012.

[7] M. Février, P. Gogol, A. Aassime, R. Mégy, C. Delacour, A. Chelnokov, A. Apuzzo, S. Blaize, J.-M. Lourtioz, and B. Dagens, "Giant coupling effect between metal nanoparticle chain and optical waveguide," *Nano Lett.*, vol. 12, no. 2, pp. 1032–1037, 2012.

[8] M. Chamanzar, Z. Xia, S. Yegnanarayanan, and A. Adibi, "Hybrid integrated plasmonic-photonic waveguides for on-chip localized surface plasmon resonance (LSPR) sensing and spectroscopy," *Opt. Express* vol. 21, no. 26, pp. 32086–32098, 2013.

[9] J. Cuadra et al. "Hybrid dielectric waveguide spectroscopy of individual plasmonic nanoparticles," *AIP Adv.*, vol. 7, 075207, 2017.

[10] N. Le Thomas, A. Dhakal, A. Raza, F. Peyskens, and R. Baets, "Impact of fundamental thermodynamic fluctuations on light propagating in photonic waveguides made of amorphous materials," *Optica*, vol. 5, no. 4, pp.328-336, 2018.

[11] B. Chen et al., "Hybrid Photon−Plasmon Coupling and Ultrafast Control of Nanoantennas on a Silicon Photonic Chip," *Nano Lett.*, vol. 18, pp. 610–617, 2018.

[12] S. M. Nie and S. R. Emery, "Probing single molecules and single nanoparticles by surface-enhanced Raman scattering," *Science*, vol. 275, pp. 1102–1106, 1997.

[13] K. Kneipp, Y. Wang, H. Kneipp, L. T. Perelman, I. Itzkan, R. R. Dasari, and M. S. Feld, "Single molecule detection using surface-enhanced Raman scattering (SERS)," *Phys. Rev. Lett.*, vol. 78, pp. 1667–1670, 1997.

[14] P. Roelli, C. Galland, N. Piro and T. J. Kippenberg, "Molecular cavity optomechanics as a theory of plasmon-enhanced Raman scattering," *Nature Nanotechnol*., vol. 11, pp. 164–169, 2016.

[15] F. Peyskens, A. Dhakal, P. Van Dorpe, N. Le Thomas, and R. Baets, "Surface enhanced Raman spectroscopy using a single mode nanophotonic-plasmonic platform," *ACS Photon.* vol. 3, no. 1, pp. 102–108, 2016.

[16] F. Peyskens, P. Wuytens, A. Raza, P. Van Dorpe and R. Baets, "Waveguide excitation and collection of surface-enhanced Raman scattering from a single plasmonic antenna," *Nanophotonics*, vol. 7, no. 7, pp. 1299–1306, 2018.

[17] A. Espinosa-Soria, A. Griol, and A. Martínez, "Experimental measurement of plasmonic nanostructures embedded in silicon waveguide gaps," *Opt. Express* vol. 24, pp. 9592-9601, 2016.

[18] A. Z. Subramanian et al.,, "Low-Loss Singlemode PECVD Silicon Nitride Photonic Wire Waveguides for 532–900 nm Wavelength Window Fabricated Within a CMOS Pilot Line," *IEEE Photon. J.*, vol. 5, pp. 2202809, 2013.

[19] R. Zhang et al., "Chemical mapping of a single molecule by plasmon-enhanced Raman scattering," *Nature*, vol. 498, pp. 82-86, 2013.

[20] F. Benz et al., "Single-molecule optomechanics in picocavities," *Science*, vol. 354, pp. 726-729, 2016.

[21] G. V. Naik, V. M. Shalaev, and A. Boltasseva, "Alternative plasmonic materials: beyond gold and silver," *Adv. Mater.*, Vol. 25, no. 24, pp. 3264–3294, 2013.

[22] G. V. Naik, J. L. Schroeder, X. Ni, A. V. Kildishev, T. D. Sands, and A. Boltasseva, "Titanium nitride as a plasmonic material for visible and near-infrared wavelengths," *Opt. Mater. Express*, vol. 2, pp. 478-489, 2012.

[23] D. Y. Fedyanin, D. I. Yakubovsky, R. V. Kirtaev, and V. S. Volkov, "Ultralow-Loss CMOS Copper Plasmonic Waveguides," *Nano Lett.* 16, 362–366 (2016)